Highlights

- 9 acylated anthocyanins (4 new) were isolated from the sprouts of *R. sativus* cv Sango
- A novel purification strategy based on orthogonal prep-LC is described
- Their structure was elucidated by combined NMR, tandem-MS and UV-Vis spectroscopies
- Their absolute reactivity with peroxyl radicals was measured for the first time
- SARs and the role of acylation for antioxidant anthocyanins are discussed on kinetic ground

Acylated anthocyanins from sprouts of *Raphanus sativus* cv. Sango: isolation, structure elucidation and antioxidant activity

Riccardo Matera[a], Simone Gabbanini[a], Serena Berretti[b], Riccardo Amorati[b], Gina Rosalinda De Nicola[c], Renato Iori[c], Luca Valgimigli[b,*]

[a] *R&D Division, BeC S.r.l., Via C. Monteverdi 49, 47122 Forlì, Italy*

[b] *Department of Chemistry ''G. Ciamician'', University of Bologna, Via S. Giacomo 11, 40126 Bologna, Italy.*

[c] *Industrial Crop Research Centre, Agricultural Research Council, (CRA-CIN), Via di Corticella, 133, 40128 Bologna, Italy*

***Corresponding author**

Luca Valgimigli: e-mail luca.valgimigli@unibo.it; Tel. +390512095683; Fax +390512095688;

Running title: Antioxidant acylated anthocyanins from Sango

Abstract

Little is known on structure-activity-relationships of antioxidant anthocyanins. *Raphanus sativus* cv Sango sprouts are among the richest sources (270 mg/100 g fresh weight). We isolated from sprouts' juice 9 acylated anthocyanins, including 4 new compounds. All comprise a cyanidin core bearing 3-to-4 glucose units, multiply acylated with malonic and phenolic acids (ferulic and sinapic). All compounds were equally effective in inhibiting the autoxidation of linoleic acid in aqueous micelles, with rate constant for trapping peroxyl radicals k_{inh} = (3.8±0.7)×10^4 $M^{-1}s^{-1}$ at 37°C. In acetonitrile solution k_{inh} varied with acylation, ranging (0.9-2.1)×10^5 $M^{-1}s^{-1}$ at 30°C; each molecule trapped a number *n* of peroxyl radicals ranging 4-to-7. Anthocyanins bearing sinapic acid were more effective than those bearing the ferulic moiety. Under identical settings, deacylated cyanin, ferulic and sinapic acids had k_{inh} of 0.4×10^5, 0.3×10^5 and 1.6×10^5 $M^{-1}s^{-1}$ respectively, with *n* ranging 2-to-3. Results show the major role of acylation on antioxidant performance.

Keywords: Anthocyanins, Phenolic acids, Radish sprouts, Peroxyl radicals, NMR, Mass spectroscopy

Chemical compounds studied in this article

Cyanidin CID 128861, Cyanin CID 441688, sinapinic acid CID 637775, ferulic acid CID 445858

1. Introduction

Anthocyanins are members of the broad flavonoid family of polyphenolic compounds and are receiving very high interest from the scientific community for their relevant health-promoting potential, related to the antioxidant activity, and for their role as functional food factors in the prevention of chronic disease (Pojer, Mattivi, Johnson, & Stockley, 2013). Their structure comprises a polyhydroxylated flavylium aglycone (the anthocyanidin) bearing one-to-several glycosidic units. In acylated anthocyanins, such glycosidic units are esterified to one-to-several organic acid residues, which often comprise phenolic acids (e.g. coumaric, ferulic, sinapic, etc.), bringing additional phenol-type hydroxyl functions to the whole structure (Figure 1). The polyphenolic structure is key to their antioxidant activity. While this property is generally accepted and studies have illustrated its relevance, *e.g.* in food preservation, mechanisms and structure-activity relationships associated to their antioxidant behaviour are far from being clarified. For example, an anthocyanin extract from rice bran was recently shown to protect emulsified fish oil from oxidation and to outperform tocols in the protection of cholesterol, although no indication was provided with regard of the structure of anthocyanins in the extract (Zhang, Shen, Prinyawiwatkul, King, & Xu, 2013). A very recent study addressed quantitative structure-activity relationships for antioxidant anthocyanins, however acylated derivatives were not investigated (Jing et al., 2014); furthermore, antioxidant performance was assessed by ORAC, a rapid assay that does not study the actual reactivity with autoxidation chain-carrying peroxyl radicals, thereby providing only an estimate of the antioxidant potential (Amorati, Foti, & Valgimigli, 2013; Roginsky & Lissi, 2005). Computational studies indicate that, among anthocyanidin cores, cyanidin that bears the catechol function in flavylium B-ring is a privileged structure with regard to its ability to trap peroxyl radicals (Guzmán, Santiago, & Sánchez, 2009), while experimental evidence suggests that glycosylation/acylation pattern has an influence on cyanidin-based antioxidants (Stintzing, Stintzing, Carle, Frei, & Wrolstad, 2002), which would reflect in their nutritional health-promoting value.

We have recently reported (Matera et al., 2012) that *Raphanus sativus* cv. Sango sprouts are among the richest sources of cyanidin-based anthocyanins (270 mg/100 g fresh weight), paralleling berries and at variance with other brassica vegetables or radish varieties, which commonly display 4-to-25-fold lower content of pigments based on the pelargonidin core (Horbowicz, Kosson, Grzesiuk, & Debski, 2008). Sango sprouts are also exceptional for the profile of cyanidin-based anthocyanins among other cyanidin sources, as we were able to distinguish 70 different structures mainly comprising polyglycosylated and polyacylated derivatives. Aiming at clarifying their healthy potential and at understanding the structure-activity relationships (SAR) for antioxidant acylated anthocyanins on solid kinetic bases, we subjected Sango sprouts juice to a fractionation procedure, using a combination of high-resolution separation techniques. We report here the isolation and structural elucidation of 9 acylated cyanidin-based anthocyanins, 4 of which have never been isolated before. Furthermore we report a preliminary kinetic investigation of their antioxidant activity, affording for the first time absolute rate constants for their reaction with peroxyl radicals. The mechanism and SAR of cyanidin-based antioxidants are preliminarily discussed.

2. Experimental

2.1. General procedures

All solvents and chemicals were from Sigma-Aldrich-Fluka (Milan, Italy) unless otherwise noted and were of the highest grade commercially available. Flash chromatography was carried out with an automatic apparatus (Combiflash™ Sg 100c, Isco Inc., Lincoln, NE, USA), equipped with a fraction collector and UV detector. Separations were achieved using C18 column RediSep® Rf Gold (50 g, particle size = 20-40 μm, 2 ∅ × 15 cm,) under a flow rate of 30 mL/min and monitoring at λ = 280 nm. The mobile phase consisted of a combination of A (aq 0.5% v/v HCOOH) and B (MeCN + 0.5% v/v HCOOH) with the following programming: t = 0, A (100%); t = 5 min, A (100%); t = 60 min, A–B (60:40 v/v); t = 75 min, A–B (60:40 v/v). Preparative and semipreparative HPLC separations were carried out on HPLC Gilson (Middleton, WI, USA) using a Rheodyne loop

of 1000 or 200 μL, respectively. The HPLC pumps were equipped with UV-Vis detector and injector/fraction collector and all the separations were dual monitored at 530 nm and 330 nm. The mobile phase for all HPLC separations consisted of a combination of A (aq 0.12% v/v TFA) and B (MeCN + 0.12% v/v TFA). Preparative chromatographic separations were achieved at room temperature on reverse phase prep-column Synergi Polar-RP (4 μm, 80 Å, 21.2 ∅ × 250 mm) (Phenomenex), with a flow rate of 20 mL/min following optimal gradient programs. Program 1 : t = 0, B (16%); t = 1 min, A (16%); t = 56 min, B (27%); t = 75 min, B (60%). Program 2: t = 0, B (18%); t = 5 min, B (18%); t = 60 min, B (29 %); t = 61 min, B (34 %), t = 65 min, B (34 %). Semi-preparative HPLC separations were obtained on Luna PFP column (5 μm, 100 Å, 10.0 ∅ × 250 mm), (Phenomenex) optimizing flow rate and gradient conditions. Roughly, the flow rate ranged 5-7.5 mL/min and gradient programs ranged t = 0, B (20-15%); t = 5 min, B (20-15%); t = 60 min, B (15-25%). Analytical HPLC was carried out on a LC-ESI-MS system (Thermo Scientific, San Jose, CA, USA) coupled to a PDA detector and equipped with a mass spectrometer LCQ Fleet® (Thermo Scientific). Analytical separation of fractions and sub-fractions was carried out at 25°C using reverse phase columns such as Synergi Polar (4 μm, 80 Å, 4.60 ∅ × 250 mm) (Phenomenex) or Hypersil GOLD PFP column (5 μm, 175 Å, 4.60 ∅ × 250 mm) (Thermo Scientific) at flow rate of 1 mL/min. Optimized gradient programs were in the range: t = 0, B (20-15%); t = 5 min, B (20-15%); t = 60 min, B (15-35%). Low resolution ESI-MS-MS^n(+) spectra were obtained by direct infusion on LCQ Fleet® mass spectrometer, following the conditions previously described (Matera et al., 2012). High Resolution mass spectra were recorded in a Thermo-Finnigan MAT95 XP instrument. NMR spectra were recorded on a Varian Inova-600 (600 MHz) spectrometer in d_6-DMSO/ CF_3COOD-d_1 (9:1). The structure of pigments was elucidated by investigation of ^1H (600 MHz) and ^{13}C (151 MHz) NMR spectra, including 2D-COSY, 2D ^1H–^{13}C HSQC and ^1H–^{13}C HMBC. The ^{13}C spectrum of pigments was completely assigned using the HSQC and HMBC experiments. Chemical shifts are reported to a TMS internal standard (δ) and coupling constant are in Hz.

2.2. Plant material, preparation and fractionation of the freeze-dried juice

Raphanus sativus (L.) cv. Sango seeds were supplied by Suba & Unico (Longiano, FC, Italy) and stored in a dry and dark place at room temperature. Seeds were identified by a lot number and guaranteed by the producer for the quality and the homogeneity of the product. The preparation and fractionation of the freeze-dried juice followed the detailed procedure already described (Matera et al., 2012). Briefly, seven days radish sprouts were squeezed to provide a dark violet juice, which was collected in liquid nitrogen and lyophilised. The obtained dark violet powder (33 g) was washed with petroleum ether (800 mL) and with acetone (800 mL) to remove lipophilic components. The remaining violet residue was suspended with 800 mL of aqueous acid solution (0.5% v/v in TFA). The pink suspension was shaken, sonicated for 5 min, and then centrifuged for 15 min at 2100g. This procedure was repeated with fresh aqueous acid solution until complete disappearance of the pink colour in the extract.

2.3. Isolation of anthocyanins

The collected aqueous extracts (0.5% v/v in TFA) were subjected to SPE through strong cation-exchange columns (Sepra-SCX, Phenomenex, 50 μm, 65 Å, 4 ∅ × 15 cm) previously conditioned with H_2O and MeCN. The elution of pigment fraction was carried out with 500 mL solution of MeCN: aq 0.1 M HCl (75:25). MeCN was removed under reduced pressure whereas the remaining water solution was lyophilized to furnish the anthocyanin-rich extract as a purple residue (1.15 g). This extract was further purified by flash chromatography, on C18 column. After MeCN removal under vacuum, the aqueous solutions were freeze-dried to give two enriched anthocyanin fractions (A= 273 mg, B= 260 mg). Fractions A and B were subjected to repeated preparative HPLC to obtain several sub-fractions that were subsequently purified on semipreparative HPLC. Isolation of pure pigments **1-9** (0.5 to 5 mg each) from eluted aqueous fractions was achieved by SPE using a C18 cartridge (Strata C18-U, 55 μm, 70 Å, 1g/6mL) previously activated with MeCN, H_2O and aq.

0.12% v/v TFA, eluting with 0.5% v/v TFA in MeOH. Methanol was removed under a gentle stream of nitrogen and the residue was dried overnight in a vacuum desiccator.

2.4 Antioxidant activity in aqueous micelles

Antioxidant activity was determined by studying the inhibited autoxidation of 30 mM linoleic acid in Triton-X100 (0.16 M) neutral micelles, in water containing 1% v/v formic acid for pH correction, which was necessary to maintain anthocyanins in the flavylium form. Autoxidation at 37 °C was initiated at constant rate R_i=6.6×10^{-9} Ms^{-1} by addition of 8.3 mM AAPH (2,2'-Azobis(2-amidinopropane)dihydrochloride). *R,R,R*-α-Tocopherol (1-5 μM) was used as reference antioxidant. Isolated anthocyanins were tested at a final concentration in the range 2-10 μM, while for anthocyanin fractions similar concentration was calculated on the average molecular weight of 1200 amu. The reaction was followed by monitoring the oxygen consumption with a miniaturized Clark-type electrode (Instech, Plymouth Meeting, PA) connected to a dual-channel amplifier Mod 203 and a A/D converter Duo.18 (World Precision Instruments, Sarasota, FL). After thermal equilibration at 37 °C of the oxidizable mixture, the appropriate amount of initiator was injected into the cell at the beginning of data collection. After a few minutes, the solution of the antioxidant was injected (Amorati, Pedulli, Cabrini, Zambonin, & Landi, 2006).

2.5 Antioxidant activity in organic solution

The absolute reactivity with peroxyl radicals was determined from kinetics of oxygen consumption during the inhibited autoxidation of 2.1 M styrene or 1.7 M cumene in MeCN (containing 1% v/v formic acid) at 30 °C (Kumar, Engman et al., 2007; Kumar, Johansson et al., 2007). The reaction was thermally initiated at constant rate (R_i in the range (2−9)×10^{-9} Ms^{-1}) by the decomposition of 2,2′-azodiisobutyronitrile (AIBN, (1−5)×10^{-2} M) and the oxygen consumption was measured in a differential oxygen-uptake apparatus based on a Validyne (Northridge, CA) DP15 pressure transducer, which has been previously described (Lucarini, Pedulli, Valgimigli, Amorati, &

Minisci, 2001). *R,R,R*-α-Tocopherol was used as reference antioxidant (Valgimigli, Lucarini, Pedulli, & Ingold, 1997). From the slope of the oxygen consumption during the inhibited period (R_{inh}), k_{inh} values were obtained by using eq. 1 (Amorati, Pedulli, & Valgimigli, 2011), where R_0 is the rate of oxygen consumption in the absence of antioxidants, $2k_t$ is the bimolecular termination rate constant of styrene or cumene (Amorati, Foti et al., 2013), and n is the stoichiometric coefficient of the antioxidant, which was determined experimentally from the length of the inhibited period (τ) by eq. 2. When the inhibited period was not clearly visible, kinetic data were confirmed by fitting the experimental traces with numerical simulations using Gepasi 3.0 software, as previously described (Amorati, Lynett, Valgimigli, & Pratt, 2012).

$$(R_0/R_{inh}) - (R_{inh}/R_0) = nk_{inh}[AH]/\sqrt{(2k_tR_i)} \quad (1)$$

$$n = \tau R_i/[AH] \quad (2)$$

3. Results and Discussion

3.1 Isolation of Anthocyanins

Preliminary HPLC analysis of the freeze-dried sprouts' juice, obtained by mechanical squeezing, revealed a very complex pattern of anthocyanins distribution, at variance with the relatively simple chromatographic profiles reported in other studies for the mature radishes of different *R. sativus* varieties (Matera et al., 2012). Therefore, we were prompted to set up a suitable isolation procedure based on the combination of SPE and high resolution chromatographic approaches. The whole anthocyanins fraction was first isolated from the freeze-dried juice. The freeze dried matrix was suspended in petroleum ether and acetone for complete removal of lipophilic compounds, then the isolation of anthocyanins was achieved by repeated extractions with aqueous acid solution (0.5% v/v in TFA). The subsequent strong-cation-exchange purification (SCX-SPE) and flash chromatography on C18 were carried out according to a previously optimized protocol (Matera et al., 2012). HPLC-MS analysis of the fraction revealed that the vast majority of components had multi-glycosylated cyanidin core, with variable acylation pattern mainly comprising phenolic acids.

In order to optimize the subsequent fractionation on preparative HPLC, we comparatively tested a number of stationary phases with higher polarity and endowed with enhanced aromatic selectivity, as compared to common C18 columns used in most published protocols. Among the tested stationary phases, the ether-linked phenyl phase (Synergi Polar-RP) endowed with additional polar groups revealed as optimal for our purpose, allowing to separate the majority of acylated anthocyanins with only few co-eluted peaks at analytical scale. After prep-HPLC fractionation, semi-preparative separations were achieved under the orthogonal pentafluorophenyl (PFP) phase, endowed with complementary electronic features. Final purification of isolated anthocyanins required one-to-two additional passages either on PFP-phase or on Synergi Polar-RP.

Overall, we were able to isolate in pure form nine acylated anthocyanins, comprising four new compounds (**1-4**) and five pigments (**5-9**) previously isolated from different botanical sources. Structures are summarized in Figure 1.

< Figure 1 about here >

*3.2 Structure elucidation of isolated anthocyanins (**1-9**)*

The structure of all anthocyanins was drafted by a combination of UV-Vis and MS^n analyses (Table 1), followed by NMR (Tables 2-3) elucidation by ^1H, homonuclear (^1H–^1H) COSY, and heteronuclear (^1H–^{13}C) HSQC and HMBC spectra, comparing to the reported data for analogous compounds. Using UV-Vis spectral features λ_{vis}, and λ_{acyl} from HPLC-DAD profiles and the relative absorbivities of **1-9** (See Table S1 in Appendix) it was possible to identify the anthocyanins as either mono- or biosides (Table 1): E_{440}/E_{vis} absorbivity ratio of 29–35% indicates a monoside (as shown by monoglycosilated cyanidin-3-glucoside, E_{440}/E_{vis}= 29 % (Fossen & Andersen, 1998)), whereas a ratio of 15–24% indicates a bioside, additionally, E_{acyl}/E_{vis} absorbivity ratio of 53–69% or 98–128% suggests monoacylation or diacylation, respectively (Arapitsas, Sjoeberg, & Turner, 2008). All anthocyanins belonged to the cyanidin family bearing the cyanidin 3-sophoroside-5-

glucoside as a common structure, variably substituted with malonic, ferulic and sinapic acids. Interestingly, three of the new pigments (**2**, **3** and **4**) bear a diglucoside pattern at the 5 position.

The five known compounds (**5-9**) were identified by spectral analyses and comparison with literature data (Idaka et al., 1987; Madhavi, Juthangkoon, Lewen, Berber-Jimenez, & L., 1996; Saito et al., 2008; Suzuki, Nagata, & Terahara, 1997; Tatsuzawa et al., 2010), as detailed in the Appendix.

The novel anthocyanin **1** ($C_{54}H_{59}O_{28}$) (Figure 1) shows absorbance percentage ratios E_{440}/E_{vis} = 17% and E_{acyl}/E_{vis} = 105% suggesting an anthocyanin bioside biacylated with two aromatic residues. The ESI(+)MS analysis exhibits the molecular ion at *m/z* 1155. CID fragmentation of *m/z* 1155 yields the ion at *m/z* 993 by loss of a glycosyl residue (162 amu) and at *m/z* 449 by loss of a diglycosyl-feruloylsinapoyl residue (706 = 324+176+206 amu). Fragmentation of *m/z* 993 in MS^3 spectrum produced the ion *m/z* 287 corresponding to the cyanidin aglycone, by loss of the 706 amu residue (Table 1). The anthocyanin **1** was presumed to be based on cyanidin-3-feruloyl-sinapoyl-diglucoside-5-glucoside and was subjected to complete NMR characterization to assign the exact connectivity of glycosyl and acyl moieties using ^{1}H, COSY, HSQC and HMBC experiments (Tables 2-3 and ^{1}H spectrum in Appendix). Three signals corresponding to the chemical shifts of acetal groups at the anomeric carbons were detected and assigned to different sugars using previously reported data for similar anthocyanins isolated in *R. sativus* (Otsuki, Matsufuji, Takeda, Toyoda, & Goda, 2002). The most downfield non-aromatic proton's signal belongs to H_1 of Glc A (δ 5.62), followed by those of Glc B (δ 5.10), and Glc C (δ 5.03). The typical diaxial coupling constants (J = 7.2-8.4 Hz) of anomeric protons of sugar residues, assigned to β-glucopyranoside in ^{1}H-NMR experiment, together HMBC correlation between H_1 of Glc B (δ 5.10) with C_2 of Glc A (δ 78.3) confirmed the typical connectivity of β-1,2 glycosidic linkage of sophorose. Literature data revealed that sophorose is always linked to C_3 position of cyanidin even though very weak HMBC correlation between the most deshielded acetalic signal belonging to H_1 of Glc A (δ 5.62) and cyanidin C_3 (δ 145.9) was observed. Moreover, HMBC correlations exist between H_1 of Glc C (δ

5.03) and C_5 of cyanidin (δ 154.6) indicating that Glc C is linked in 5-position of cyanidin. The exact connectivity pattern of sugar residues was obtained by ^{1}H and COSY experiments and by comparing with literature data (Otsuki et al., 2002). Proton signals from sinapic acid residue (R_3) were observed at δ 7.42, 6.88, 6.40, which correlated with the singlet at δ 3.75, integrating for six protons. Furthermore, HMBC correlation exists between H_2 of Glc B (δ 4.60) and carbon signal of sinapic acid carbonyl (δ 166.3). Two geminal methylene protons H_{6a} and H_{6b} of Glc B (δ 4.25 and 4.32) showed a downfield shift indicating that this position is acylated with ferulic acid (R_2) as demonstrated by HMBC correlations with ferulic carbonyl (δ 165.6). The cinnamic residues were elucidated as *trans* based on the large coupling constants (J = 15-16 Hz) of the α and β protons of ferulic and sinapic moieties. Moreover, HMBC correlations between proton signals of 3-OCH_3 (δ 3.70) and C_3 (δ 147.6) of the feruloyl group proceed through stepwise $^3J_{CH}$ up to the carbonyl (δ 165.6) of ferulic group. Similarly, observed HMBC correlations between the 3-OCH_3 and 5-OCH_3 proton signal (δ 3.75) up to the carbonyl (δ 166.3) of sinapoyl group allow to discriminate the remaining signals related to each cinnamic moiety by crossing data from HMBC, HSQC and COSY experiments. Therefore, the novel anthocyanin **1** was identified as cyanidin 3-*O*-[2-*O*-(2-*O*-(*E*)-sinapoyl-6-*O*-(*E*)-feruloyl-β-D-glucopyranosyl)-β-D-glucopyranoside]-5-*O*-(β-D-glucopyranoside).

The novel anthocyanin **2** ($C_{63}H_{71}O_{36}$) (Figure 1) shows a percentage ratio E_{440}/E_{vis} of 23% suggesting an anthocyanin bioside, while the ratio E_{acyl}/E_{vis} of 98% suggests biacylation with two aromatic residues. The ESI(+)MS analysis showed *m/z* 1403 as molecular ion. MS^2 fragmentation of *m/z* 1403 revealed the three main ions (*m/z* 1359, *m/z* 993 and *m/z* 697) originating by loss of carbon dioxide (44 amu), malonoyl-diglucoside (410 amu) and the diglycosyl-feruloylsinapoyl (706 amu) residues, respectively. MS^3 fragmentation of each ion produced the cyanidin aglycone fragment at *m/z* 287 (Table 1). The anthocyanin **2** was presumed to be based on cyanidin-3-feruloyl-sinapoyl-diglucoside-5-malonoyl-diglucoside and was subjected to full NMR characterization (^{1}H, COSY, HSQC and HMBC) (Tables 2-3 and ^{1}H spectrum in Appendix). Four signals corresponding to the chemical shifts of acetalic groups at the anomeric carbons were detected and assigned to

different sugars using previously reported data: the acetalic proton's signal shifted at the lowest field (δ 5.60) belongs to the H_1 of Glc A, then signals at higher field belong to Glc B (δ 5.13), and Glc C (δ 5.21), respectively. The doublet of the acetalic proton shifted at the highest field (δ 4.27) belongs to Glc D. The exact connectivity pattern of sugar residues was obtained by ^{1}H and COSY experiments. The typical diaxial coupling constants (J = 7.1-7.8 Hz) of anomeric protons of sugar residues shown in ^{1}H-NMR experiments, which was assigned to β-glucopyranoside, together with the HMBC correlation between H_2 of Glc A (δ 4.12) with C_1 of Glc B (δ 99.7), confirmed the typical connectivity of β-1,2 glycosidic linkage of sophorose. This is linked to C_3 position of cyanidin even though a very weak HMBC correlation appears between the most deshielded acetalic signal belonging to H_1 of Glc A (δ 5.60) and cyanidin C3 (δ 144.9). Four couples of methylene protons belong to C_6 positions of each glucose as confirmed by HSQC correlations, together with an additional cross peak indicating the methylene of malonic acid (R_4) (δ 3.30). The deshielded signals of geminal protons H_{6a} e H_{6b} of Glc A and Glc C refer to positions acylated with ferulic (R_1) and malonic acid (R_4), respectively, as confirmed by the weak HMBC correlation between ferulic ester carbonyl (δ 166.8) and two geminal protons, H_{6a} e H_{6b}, of Glc A (δ 4.21 and 4.36), together with a correlation between the malonic ester carbonyl (δ 166.7) and two protons, H_{6a} e H_{6b}, of Glc C (δ 4.26 and 4.39). Proton signals from sinapic acid (R_3) were observed at δ 7.43, 6.91, 6.46, which correlated with a singlet (δ 3.78) integrating for six protons. Furthermore, HMBC correlation exists between proton at H_2 of Glc B (δ 4.64) and the carbonyl (δ 166.2) of sinapic acid. The cinnamic residues' configuration was elucidated as *trans* due to the large coupling constants (J = 16.2 Hz). By means of HMBC analysis, $^3J_{CH}$ stepwise correlations were observed from olefinic ferulic protons at α and β position (δ 6.24 and 7.33, respectively) up to the proton signal of 3-OCH_3 (δ 3.71) and the C_3 (δ 148.4) of the ferulic acid. Similarly, HMBC correlation is observed between the 3-OCH_3 and 5-OCH_3 proton signal (δ 3.78) and the carbon signal at the C_3 and C_5 (δ 148.5) of sinapic acid. Crossing data from HMBC, HSQC and COSY allowed distinguishing all signals related to ferulic and sinapic acid. The complete data set for this anthocyanin is very similar to the

known compound **5** (See Appendix), except for the signals related to the additional Glc D. Due to the paucity of material analyzed, no HMBC correlations were observed between Glc C and Glc D because the intrinsic difficulty with observing $^{3}J_{CH}$ in flexible cycles like glycosides even at lower temperature (15 °C). For this reason, in this study we refer to the structure elucidation of a very similar acylated pelargonidin isolated from rhizome of *R. sativus*, based on β-1,4 diglucoside, recently published by Mori and coworkers (Mori, Nakagawa, Maeschima, Niiura, & Yoshida, 2006) due to the identity of the vegetal species. Therefore, the novel anthocyanin **2** was identified as cyanidin 3-*O*-[6-*O*-(*E*)-feruloyl-2-*O*-(2-*O*-(*E*)-sinapoyl-β-D-glucopyranosyl)-β-d-glucopyranoside]-5-*O*-(4-*O*-β-D-glucopyranosyl-6-*O*-malonoyl-β-D-glucopyranoside).

The novel anthocyanin **3** ($C_{62}H_{69}O_{35}$) (Figure 1) shows very similar UV-Vis and MS^n properties as anthocyanin **2**. The ESI(+)MS analysis shows *m/z* 1373 as molecular ion suggesting it to be acylated with two ferulic acids (Table 1). The spectral data of both compounds were very similar: the ^{1}H and ^{13}C NMR spectra (Table 2) revealed that **2** and **3** have feruloyl and sinapoyl groups, and two feruloyl groups, respectively. The connectivities of the glycosides, malonic residue and two acyl groups in **2** and **3** were equivalent as confirmed by HMBC analysis and were referred to a similar acylated pelargonidin isolated by Mori and coworkers from *R. sativus* (Mori et al., 2006). Therefore, the novel anthocyanin **3** was identified as cyanidin 3-*O*-[6-*O*-(*E*)-feruloyl-2-*O*-(2-*O*-(*E*)-feruloyl-β-D-glucopyranosyl)-β-D-glucopyranoside]-5-*O*-(4-*O*-β-D-glucopyranosyl-6-*O*-malonoyl-β-D-glucopyranoside) (see complete structure elucidation in Appendix)

The novel anthocyanin **4** ($C_{62}H_{69}O_{35}$) (Figure 1) shows almost identical UV-Vis and MS^n properties as anthocyanin **3**. The ESI(+)MS analysis shows *m/z* 1373 as molecular ion suggesting it to be acylated with two ferulic acids (Table 1). The spectral data of anthocyanins **3** and **4** were similar: the ^{1}H (Table 2) and COSY revealed both compounds share two feruloyl groups. The connectivities of the glycosides, the malonic residue and two ferulic groups in **3** and **4** differentiate only for the acylation site as revealed by the downfield shifted signals of methylene protons of H_6 of Glc B (δ 4.27), which indicate the ferulic acid (R_2) acylation. The ^{1}H-NMR data set of anthocyanin

is very similar to compound **9** (see details in Appendix), except for the signals related to the additional Glc D. In the absence of sufficiently intense ^{13}C signals (not listed in table 3) the connectivity between Glc C and Glc D was referred to the work by Mori and coworkers on *R. sativus* (Mori et al., 2006). Therefore, the novel anthocyanin **4** was identified as cyanidin 3-*O*-[6-*O*-(*E*)-feruloyl-2-*O*-(6-*O*-(*E*)-feruloyl-β-D-glucopyranosyl)-β-D-glucopyranoside]-5-*O*-(4-*O*-β-D-glucopyranosyl-6-*O*-malonoyl-β-D-glucopyranoside) (see complete structure elucidation in Appendix)

3.3 Antioxidant activity of isolated anthocyanins in aqueous micelles

The study of the inhibited autoxidation of an oxidizable substrate under controlled conditions is the golden standard in antioxidant testing, as it challenges the performance of antioxidants in close-to-real model systems and directly evaluates the ability of the antioxidant to trap peroxyl radicals, which are responsible for oxidative chain-carrying (Amorati, Foti et al., 2013; Valgimigli et al., 1997; Valgimigli & Pratt, 2012). Therefore, we investigated the ability of isolated anthocyanins to protect linoleic acid, incorporated in aqueous neutral micelles, from autoxidation induced by controlled thermal decomposition of water soluble azo-initiator AAPH at 37°C. Since previous knowledge indicated that the antioxidant behaviour of anthocyanins depends on pH and that the characteristic flavylium form is only prevailing under acidic conditions, we added 1% formic acid in all experiments and verified the presence of the flavylium form by UV-Vis spectrophotometry. Any of the tested pigments afforded good antioxidant protection, significantly reducing the rate of autoxidation already when used at micromolar levels, and the inhibition was proportional to the concentration, as shown in Figure 2A. However the performance was sensibly lower than that offered under similar settings by reference α-tocopherol, which gave almost complete inhibition of oxygen consumption for an inhibited period (τ) that lasted until complete consumption of the antioxidant. Interestingly, the apparent antioxidant performance was identical for any tested anthocyanin, irrespective of the degree and type of acylation/glycosylation. For anthocyanins **1-9**

the apparent rate constant for peroxyl radical trapping in aqueous micelles, obtained by processing oxygen consumption plots with equation (1), was in the range k_{inh}=(3.8±0.7)×10^4 $M^{-1}s^{-1}$, as compared to the value of (6.1±0.3)×10^5 $M^{-1}s^{-1}$ recorded for α-tocopherol. Indeed, when we tested a semi-purified fraction (fraction 8, see Appendix) containing about 13 main anthocyanins differing for the pattern of acylation/glycosylation, again we obtained the same antioxidant performance. Basic hydrolysis of the fraction (to remove acylating units) did not significantly alter the antioxidant activity (Appendix). This behaviour apparently suggests that the presence of acylating phenolic acids and the actual acylation/glycosylation pattern have little influence on the antioxidant performance, which must come entirely from the cyanidin. This conclusion, however, would conflict with previous experimental evidence (Stintzing et al., 2002), and would be counterintuitive, considering that phenolic acids (the acylating units) have long been considered good antioxidants (Amorati et al., 2006; Foti, Piattelli, Baratta, & Ruberto, 1996; Kikuzaki, Hisamoto, Hirose, Akiyama, & Taniguchi, 2002). A reasonable explanation for the observed behaviour is that the reactivity of water soluble anthocyanins, residing outside the micelle lipid core, with lipid soluble peroxyl radicals, formed during autoxidation of linoleic acid inside the lipid core, is mainly regulated by the exchange of antioxidant inside/outside the micelle. Therefore, the protective activity of the antioxidant is limited by its ability to access the micelle, which favours lipid soluble α-tocopherol and disfavour anthocyanins, whose partition is only marginally affected by their acylation pattern. This finding is in line with previous observation that the antioxidant activity of phenolic acids and related compounds in heterogeneous media is influenced by their O/W partition coefficient (Foti et al., 1996; Kikuzaki et al., 2002).

3.4. Antioxidant activity in homogenous solution

To gain knowledge on the absolute reactivity of anthocyanins with peroxyl radicals and draw structure-activity relationships on reliable kinetic ground, we turned to homogenous organic solution, and studied the inhibited autoxidation of cumene and styrene in MeCN at 30°C. Although

they are not biomimetic substrates, cumene and styrene are, by far, the best known model systems in autoxidation studies and provide complementary information (Amorati, Valgimigli, Panzella, Napolitano, & d'Ischia, 2013). Due to limited availability of purified material, we focused our kinetic measurements on anthocyanins **5**, **7**, **8**, **9,** together with their acylating acids, de-acylated cyanin (bearing glucose A and C bound to the cyanidin core) and α-tocopherol as reference antioxidant. As previously discussed, formic acid was added to the solutions to maintain the anthocyanin in the flavylium form.

In the controlled autoxidation of cumene (Figure 2B), characterized by a modest oxidizability (the propagation rate constant for oxidative chain is k_p=0.34 $M^{-1}s^{-1}$ at 30 °C, while the corresponding value for linoleic acid is k_p=62 $M^{-1}s^{-1}$ (Valgimigli & Pratt, 2012)), any of the tested anthocyanins gave complete inhibition already at micromolar level, until all the antioxidant was consumed. Although this prevented distinguishing the performance of the different anthocyanins, it allowed the accurate determination of the stoichiometric factor, *n*, *i.e.* the number of peroxyl radicals trapped by one molecule of antioxidant. Common phenolic antioxidants are expected to trap two peroxyl radicals per molecule (n = 2): this was indeed the case for α-tocopherol, for isolated phenolic acids (ferulic and sinapic) or for their simple esters, as summarized in table 4. Cyanin had n ~ 3 suggesting that, beside the catechol moiety expected to trap two peroxyl radicals (Amorati & Valgimigli, 2012), also the free OH function in 7 position contributes to some extent to the antioxidant activity. Interestingly all tested anthocyanins had much larger stoichiometric factors, ranging from n ~ 4 for anthocyanin **8** bearing one ferulic acid residue, to about 6-7 for anthocyanins **5**, **7** and **9** bearing two phenolic acids (sinapic or ferulic). This indicated a nearly additive contribution of the antioxidant behaviour of the different moieties, each phenolic acid trapping approximately two peroxyl radicals and the aglycone trapping two-to-three peroxyl radicals. Hence, each acylated anthocyanin outperformed α-tocopherol in terms of duration of the antioxidant effect, which largely depended on the degree of acylation.

In the autoxidation of more oxidizable styrene (k_p=41 $M^{-1}s^{-1}$, close to linoleic acid (Amorati et al., 2012)), it was instead possible to sharply differentiate the variable antioxidant performance of diverse anthocyanins and their main moieties, as shown in figure 2C. As expected, reference α-tocopherol gave a neat inhibited period, whose length corresponded to n = 2, followed by the re-onset of uninhibited oxygen uptake after antioxidant consumption. Acylated anthocyanins had instead a different behaviour: they gave and initial inhibited period of length corresponding to n ~ 2-4, followed by a retarded period, where the autoxidation was not fully inhibited yet it was significantly slower that in the absence of an antioxidant (Figure 2C).

This indicated that different antioxidant sites of the anthocyanin molecule have diverse ability in trapping peroxyl radicals (Kumar et al., 2010), although the different sites cannot be distinguished in the autoxidation of cumene, resulting in a unique longer inhibited period. Analysis of the specific portions of oxygen uptake plots by means of equation (1) allowed to obtain the apparent rate constant for peroxyl radical trapping of the different active moieties, as summarized in Table 4. Focusing on the first inhibited period, anthocyanins **5** and **7** bearing the sinapic residue gave significantly higher inhibition rate constants (k_{inh} ~ 2×10^5 $M^{-1}s^{-1}$), and comparison with the measured k_{inh} values for sinapic acid and its methyl ester suggests that such residue is the main contributor to their antioxidant performance. Indeed de-acylated cyanin showed only k_{inh} = 4×10^4 $M^{-1}s^{-1}$, identical to the value recorded for ferulic acid or its ethyl ester. Anthocyanins **8** and **9** bearing one and two ferulic acids residues, respectively, had somewhat intermediate antioxidant performance, with k_{inh} ranging 0.9-1.2×10^5 $M^{-1}s^{-1}$, thereby suggesting some positive interference between one ferulic acid residue and the cyanidin moiety (Amorati & Valgimigli, 2012). Analysis of the subsequent retarded period in oxygen uptake plots provided a second inhibition rate constant k_{inh} ~ 3-4×10^4 $M^{-1}s^{-1}$ for any acylated anthocyanin, *i.e.* corresponding to the antioxidant performance of the glycosylated cyanidin or one ferulic acid residue.

Taken together, data suggest that the most active molecular site is sinapic acid, when present, which is able to trap two peroxyl radicals by formal H-atom transfer and to interact with the cyanidin

residue, *e.g.* by hydrogen exchange with the catechol moiety. For this reason, an extended duration of inhibition is observed, trapping 3-4 peroxyl radicals with maximum efficiency. The mechanistic and thermodynamic basis of analogous synergic interaction occurring intermolecularly in antioxidant mixtures has recently been discussed (Valgimigli et al., 2013). Similarly, a synergic interaction between the ferulic residue and the cyanidin moiety is responsible for the (somewhat less effective) fast antioxidant response of anthocyanins bearing only ferulic acid residues. In all cases additional antioxidant functions are left on the anthocyanin, namely the (second) ferulic acid residue or the unblocked hydroxyl functions on the cyanidin core, which will trap additional peroxyl radicals with a lower, yet relevant, rate constant, thereby extending the overall antioxidant performance.

4. Conclusions

By means of a novel fractionation approach we have isolated and characterized nine acylated anthocyanins from the sprouts juice of *R. sativus* cv Sango, which share the cyanidin core and bear three-to-four glycosidic residues acylated with malonic, ferulic and sinapic acids. Four new compounds were characterized for the first time. All compounds had similar antioxidant activity in aqueous micelles, while their performance differentiated in homogenous organic solution. Acylation pattern significantly affected their antioxidant performance and pigments bearing a sinapic acid moiety were the most effective, approaching the reactivity of reference α-tocopherol in quenching peroxyl radicals. Every tested compound outperformed α-tocopherol in terms of number of peroxyl radicals trapped by each antioxidant molecule. This is the first investigation providing absolute peroxyl-radical-trapping kinetics of acylated anthocyanins and highlighting the distinctive contribution of the different structural moieties in the antioxidant performance. Hopefully our results will help rationalize their structure-activity relationships. They highlight the importance of acylation/glycosylation pattern of anthocyanins in determining their healthy-nutritional value.

Acknowledgements

Financial support from BeC S.r.l. (Forlì, Italy), the University of Bologna (Italy) , CRA-CIN (Bologna, Italy), MIUR (Italy) PRIN 2010-2011 2010PFLRJR (PROxi project) and COST Action CM1201 (Biomimetic Radical Chemistry).

Appendix. Supplementary data

Supplementary data associated with this article can be found, in the online version, at ….

References

Amorati, R., Foti, M. C., & Valgimigli, L. (2013). Antioxidant activity of essential oils. *J Agric Food Chem, 61*, 10835-10847.

Amorati, R., Lynett, P. T., Valgimigli, L., & Pratt, D. A. (2012). The reaction of sulfenic acids with peroxyl radicals: insights into the radical-trapping antioxidant activity of plant-derived thiosulfinates. *Chem Eur J, 18*, 6370 – 6379.

Amorati, R., Pedulli, G. F., Cabrini, L., Zambonin, L., & Landi, L. (2006). Solvent and pH effects on the antioxidant activity of caffeic and other phenolic acids. *J Agric Food Chem, 54*, 2932-2937.

Amorati, R., Pedulli, G. F., & Valgimigli, L. (2011). Kinetic and thermodynamic aspects of the chain-breaking antioxidant activity of ascorbic acid derivatives in non-aqueous media. *Org Biomol Chem, 9*, 3792-3800.

Amorati, R., & Valgimigli, L. (2012). Modulation of the antioxidant activity of phenols by non-covalent interactions. *Org Biomol Chem, 10*, 4147-4158.

Amorati, R., Valgimigli, L., Panzella, L., Napolitano, A., & d'Ischia, M. (2013). 5-S-Lipoylhydroxytyrosol, a multidefense antioxidant featuring a solvent-tunable peroxyl radical-scavenging 3-thio-1,2-dihydroxybenzene motif. *J Org Chem, 78*, 9857−9864.

Arapitsas, P., Sjoeberg, P. J. R., & Turner, C. (2008). Characterisation of anthocyanins in red cabbage using high resolution liquid chromatography coupled with photodiode array detection and electrospray ionization-linear ion trap mass spectrometry. *Food Chem, 109*, 219-226.

Fossen, T., & Andersen, Ø. M. (1998). Cyanidin 3-O-(6″-succinyl-β-glucopyranoside) and other anthocyanins from *Phragmites australis*. *Phytochemistry, 49*, 1065-1068.

Foti, M. C., Piattelli, M., Baratta, M. T., & Ruberto, G. (1996). Flavonoids, coumarins, and cinnamic acids as antioxidants in a micellar system. Structure-activity relationship. *J Agric Food Chem, 44*, 497-501.

Guzmán, R., Santiago, C., & Sánchez, M. (2009). A density functional study of antioxidant properties on anthocyanidins. *J Mol Struct, 935*, 110-114.

Horbowicz, M., Kosson, R., Grzesiuk, A., & Debski, H. (2008). Anthocyanins of fruits and vegetables - their occurrence, analysis and role in human nutrition. *Veget Crops Res Bull, 68*, 5-22.

Idaka, E., Yamakita, H., Ogawa, T., Kondo, T., Yamamoto, M., & Goto, T. (1987). Structure of three diacylated anthocyanins isolated from red cabbage, *Brassica oleracea*. *Chem Lett*, 1213-1216.

Jing, P., Zhao, S., Ruan, S., Sui, Z., Chen, L., Jiang, L., & Qian, B. (2014). Quantitative studies on structure-ORAC relationships of anthocyanins from eggplant and radish using 3D-QSAR. *Food Chem, 145*, 365-371.

Kikuzaki, H., Hisamoto, M., Hirose, K., Akiyama, K., & Taniguchi, H. (2002). Antioxidant properties of ferulic acid and its related compounds. *J Agric Food Chem, 50*, 2161-2168.

Kumar, S., Engman, L., Valgimigli, L., Amorati, R., Fumo, M. G., & Pedulli, G. F. (2007). Antioxidant profile of ethoxyquin and some of its S, Se, and Te analogues. *J Org Chem, 72*, 6046-6055.

Kumar, S., Johansson, H., Engman, L., Valgimigli, L., Amorati, R., Fumo, M. G., & Pedulli, G. F. (2007). Regenerable chain-breaking 2,3-dihydrobenzo[b]selenophene-5-ol antioxidants. *J Org Chem, 72*, 2583-2595.

Kumar, S., Johansson, H., Kanda, T., Engman, L., Muller, T., Bergenudd, H., Jonsson, M., Pedulli, G. F., Amorati, R., & Valgimigli, L. (2010). Catalytic chain-breaking pyridinol antioxidants. *J Org Chem, 75*, 716–725.

Lucarini, M., Pedulli, G. F., Valgimigli, L., Amorati, R., & Minisci, F. (2001). Thermochemical and kinetic studies of a bisphenol antioxidant. *J Org Chem, 66*, 5456-5462.

Madhavi, D. L., Juthangkoon, S., Lewen, K., Berber-Jimenez, M. D., & L., S. M. A. (1996). Characterization of anthocyanins from *Ajuga pyramidalis Metallica Crispa* cell cultures. *J Agric Food Chem, 44*, 1170-1176.

Matera, R., Gabbanini, S., De Nicola, G. R., Iori, R., Petrillo, G., & Valgimigli, L. (2012). Identification and analysis of isothiocyanates and new acylated anthocyanins in the juice of *Raphanus sativus* cv. Sango sprouts. *Food Chem, 133*, 563-572.

Mori, M., Nakagawa, S., Maeschima, M., Niiura, S., & Yoshida, K. (2006). Anthocyanin from the rhizome of *Raphanus sativus*, and change in the composition during maturation. *Heterocycles, 69*, 239-251.

Otsuki, T., Matsufuji, H., Takeda, M., Toyoda, M., & Goda, Y. (2002). Acylated anthocyanins from red radish (*Raphanus sativus L.*). *Phytochemistry, 60*, 79-87.

Pojer, E., Mattivi, F., Johnson, D., & Stockley, C. S. (2013). The case for anthocyanin consumption to promote human health: a review. *Compr Rev Food Sci Food Saf, 12*, 483-508.

Roginsky, V., & Lissi, E. A. (2005). Review of methods to determine chain-breaking antioxidant activity in food. *Food Chem, 92*, 235-254.

Saito, N., Tatsuzawa, F., Suenaga, E., Toki, K., Shinoda, K., Shigihara, A., & Honda, T. (2008). Tetra-acylated cyanidin 3-sophoroside-5-glucosides from the flowers of *Iberis umbellata L.* (Cruciferae). *Phytochemistry, 69*, 3139-3150.

Stintzing, F. C., Stintzing, A. S., Carle, R., Frei, B., & Wrolstad, R. E. (2002). Color and antioxidant properties of cyanidin-based anthocyanin pigments. *J Agric Food Chem, 50*, 6172-6181.

Suzuki, M., Nagata, T., & Terahara, N. (1997). New acylated anthocyanins from *Brassica campestris var. chinensis*. *Biosci Biotech Biochem, 61*, 1929-1930.

Tatsuzawa, F., Saito, N., Toki, K., Shinoda, K., Shigihara, A., & Honda, T. (2010). Acylated cyanidin 3-sophoroside-5-glucosides from the purple roots of red radish (*Raphanus sativus L.*) 'Benikanmi'. *J Jpn Soc Hortic Sci, 79*, 103-107.

Valgimigli, L., Bartolomei, D., Amorati, R., Haidasz, E., Hanthorn, J. J., Nara, S. J., Brinkhorst, J., & Pratt, D. A. (2013). 3-Pyridinols and 5-pyrimidinols: Tailor-made for use in synergistic radical-trapping co-antioxidant systems. *Beilstein J Org Chem, 9*, 2781–2792.

Valgimigli, L., Lucarini, M., Pedulli, G. F., & Ingold, K. U. (1997). Does beta-carotene really protect vitamin E from oxidation? *J Am Chem Soc, 119*, 8095-8096.

Valgimigli, L., & Pratt, D. A. (2012). Antioxidants in chemistry and biology. In C. Chatgilialoglu & A. Studer (Eds.), *Encyclopedia of Radicals in Chemistry, Biology and Materials.* (Vol. 3, pp. 1623-1678). Chirchester (UK): John Wiley & Sons.

Zhang, X., Shen, Y., Prinyawiwatkul, W., King, J. M., & Xu, Z. (2013). Comparison of the activities of hydrophilic anthocyanins and lipophilic tocols in black rice bran against lipid oxidation. *Food Chem, 141*, 111-116.

Figures and Tables Legend

Figure 1. Structures of the anthocyanins isolated from *Raphanus sativus* cv. Sango sprouts.

Figure 2. Oxygen uptake kinetics during the controlled autoxidation of: A) 30 mM linoleic acid in Triton-X100 (0.16 M) neutral micelles at 37°C without inhibitor (a), or inhibited by: anthocyanin **1**, 4.0 μM (b), or 8.0 μM (c); anthocyanin **3**, 4.0 μM (d), or 8.0 μM (e); 3.3 μM α-tocopherol (f); B) 1.7 M cumene in acetonitrile at 30°C without inhibitor (a), or inhibited by: 5.5 μM anthocyanin **8** (b); 4.5 μM anthocyanin **7** (c); 3.9 μM anthocyanin **5** (d). C) 2.1 M styrene in acetonitrile at 30°C without inhibitor (a), or inhibited by: 5.0 μM Ethyl ferulate (b); 6.0 μM α-tocopherol (c); 4.2 μM anthocyanin **7** (d). Dashed lines represent linear regressions of the inhibited and subsequent portion of autoxidation; τ indicates the inhibition time.

Table 1. HR-ESI(+)MS**,** ESI (+)-MS/MS^n and UV-Vis spectroscopic data for anthocyanins isolated from *R. sativus* cv. Sango.

Table 2. ^{1}H NMR spectroscopic data of anthocyanins isolated from *R. sativus* cv. Sango sprouts in DMSO-d_6 : TFA-d_1 (9:1).

Table 3. ^{13}C NMR spectroscopic data of anthocyanins isolated from *R. sativus* cv. Sango sprouts in DMSO-d_6 : TFA-d_1 (9:1) . Signals were indirectly detected by HSQC and HMBC analysis.

Table 4. Rate constants and stoichiometric factors for reaction with peroxyl radicals of anthocyanins from *R. sativus* cv. Sango sprouts, their acylating phenolic acids and corresponding esters, and reference compounds, determined from the inhibited autoxidation of styrene and cumene in acetonitrile (containing 1% v/v formic acid) at 30°C.

Table 1. HR-ESI(+)MS**,** ESI (+)-MS/MS^n and UV-Vis spectroscopic data for anthocyanins isolated from *R. sativus* cv. Sango.

ID	Molecular formula	HR-ESI(+) MS found (calculated)	ESI $[M]^+$	MS tandem[a]			UV-Vis spectral properties[b]			
				MS^2 ions	MS^3 ions	MS^4 ions	λ_{acyl} max [nm]	λ_{vis} max [nm]	Acylation ratio (%)[c]	Glycosylation ratio (%)[d]
1	$C_{54}H_{59}O_{28}$	1155.3199 (1155.3187)	1155	**993** (100), 449 (30)	287 (100)		329	535	105	17
2	$C_{63}H_{71}O_{36}$	1403.3725 (1403.3720)	1403	1359 (20)**, 993** (100), 697 (75)	993 (70), 287 (100)		330	535	98	23
3	$C_{62}H_{69}O_{35}$	1373.3631 (1373.3614)	1373	1329 (25), 963 (100), **697** (90)	697 (100), 653 (10), 287 (70)		329	535	98	18
4	$C_{62}H_{69}O_{35}$	1373.3627 (1373.3614)	1373	1329 (20), **963** (100), 697 (10)	**963** (5), 625 (10), 287 (100)	287 (100)	328	534	107	16
5	$C_{57}H_{61}O_{31}$	1241.3184 (1241.3191)	1241	**1197** (20), 993 (70), 535 (100)	**993** (100), 491 (60),	287 (100)	329	533	99	17
6	$C_{44}H_{51}O_{25}$	979.2720 (979.2714)	979	979 (10) 817 (100) **449** (30) 287	287 (100)		334	527	58	18
7	$C_{54}H_{59}O_{28}$	1155.3175 (1155.3187)	1155	**993** (100), 449 (10)	993 (70), 287 (100)		329	533	128	22
8	$C_{46}H_{51}O_{27}$	1035.2619 (1035.2612)	1035	787 (70), **535** (100)	287 (100)		327	522	53	18
9	$C_{56}H_{59}O_{30}$	1211.3098 (1211.3086)	1211	1167 (20), **963** (100), 535 (70)	287 (100)		328	530	110	18

[a] Relative intensities of each ion are in parentheses; the most abundant ion (in bold) is selected for subsequent fragmentation.
[b] Evaluated by HPLC-DAD on Hypersil GOLD PFP column (5 μm, 175 Å, 4.6 × 250 mm) eluting with A (aq 0.12% v/v TFA) and B (MeCN + 0.12% v/v TFA). See gradient program on the text.
[c] Acylation ratio = E_{acyl}/E_{vis}, 59–63% indicates monoacylation, 98–128% indicates diacylation.
[d] Glycosylation ratio = E_{440}/E_{vis}, 15–24% indicates bioside, 29–35% indicates monoside.

Table 2. ^{1}H NMR spectroscopic data of anthocyanins isolated from *R. sativus* cv. *Sango* sprouts in DMSO-d_6 : TFA-d_1 (9:1)[a]

	1	**2**	**3**	**4**	**5**	**6**	**7**	**8**	**9**
Cyanidin									
4	8.69 s	8.71 s	8.71 s*	8.77 s	8.73 s	8.83 s	8.74 s	8.73 s	8.78
6	7.02 s	6.94 s	6.90 s	7.04 s	6.91 s	6.92 s	6.93 s	6.91 s	6.91 s
8	6.89 s	6.90 s	6.88 s	6.88 s	6.91 s	6.97 s	6.88 s	6.98 s	6.91 s
2’	7.85 d (2.4)	7.89 s	7.87 s	7.97 s	7.88 d (1.8)	7.92 s	7.89 s	7.99 d (2.4)	7.90 s
5’	7.07 d (9.0)	7.10 d (8.4)	7.01 d (8.8)	7.05 d*	7.11 d (9.0)	7.10 d (8.8)	7.11 d (8.4)	7.04 d (8.4)	7.07 m*
6’	8.31 dd (9.0, 1.8)	8.34 d (8.4)	8.30 d (8.8)	8.21 d (8.4)	8.33 dd (9.0, 2.2)	8.34 d (8.8)	8.33 d (8.4)	8.20 dd (8.4, 2.4)	8.23 (8.4)
Glc A									
1	5.62 d (7.2)	5.60 d (6.6)	5.58 d (7.2)	5.58 d (7.2)	5.64 d (7.2)	5.51 d (7.6)	5.66 d (7.2)	5.61 d (7.2)	5.62 d (7.3)
2	4.07 t (7.8)	4.12 d (7.8)	4.10 t (7.6)	4.00 m	4.12 t (7.8)	4.03 t (8.0)	4.12 t (8.2)	4.06 t (8.0)	4.01 t (7.9)
3	3.61 t (8.4)	3.65 m *	3.64 m*	3.85 m*	3.65 m*	3.68 m*	3.64 t (7.8)	3.67 m *	3.70 m*
4	3.60 m*	3.45 m *	3.45 m*	3.88 m*	3.45 m*	3.40 m*	3.49 m*	3.35 m *	3.45 m*
5	3.65 m*	3.93 m *	3.97 m*	3.98 m*	3.94 m*	3.30 m*	3.91 m	3.97 m	3.91 m*
6a	3.86 m*	4.21 m *	4.27 m*	4.21 m*	4.18 dd (12.6, 5.8)	3.40 m*	4.23 dd (11.2, 5.6)	4.28 m	4.20 d (11.9)
6b	3.60 m*	4.36 d (12.0)	4.37 m*	4.30 m*	4.39 m*	3.40 m*	4.34 d (11.2)	4.44 d (10.2)	4.41 d (11.9)
Glc B									
1	5.10 d (7.8)	5.13 d (7.8)	5.12 d (8.0)	4.70 d (7.2)	5.15 d (8.4)	5.13 d (7.6)	5.14 d (8.2)	4.61 d (7.8)	4.78 d (7.7)
2	4.60 t (9.0)	4.64 t (7.8)	4.64 t (8.0)	3.10 m*	4.65 t (8.4)	4.60 t (8.8)	4.67 t (8.5)	2.94 t (8.7)	3.10 m *
3	3.44 m*	3.35 m *	3.35 m*	3.15 m*	3.37 m*	3.70 m*	3.37 t (9.0)	3.06 t (9.0)	3.21 m*
4	3.40 m*	3.14 m *	3.16 m*	3.20 m*	3.16 m*	3.40 m*	3.15 t (9.0)	2.99 t (9.0)	3.35 m*
5	3.35 m*	3.04 m*	3.03 m*	3.08 m*	3.05 t (7.2)	3.30 m*	3.08 t (8.5)	2.67 m	3.61 m *
6a	4.25 m	3.39 m *	3.38 m*	4.27 m*	3.41 m*	3.40 m*	3.60 m*	3.11 m *	3.89 m*
6b	4.32 m	3.63 m *	3.60 m*	4.27 m*	3.65 m*	3.40 m*	3.40 m*	3.15 m *	4.01 m *
Glc C									
1	5.03 d (7.2)	5.21 (6.0)	5.19 d (7.0)	5.07 d (7.6)	5.13 d (7.2)	5.07 d (7.6)	5.06 d (7.5)	5.10 d (7.2)	5.06 d (7.8)

2	3.47 m	3.57 m *	3.56 m*	3.59 m*	3.52 m*	3.55 m*	3.50 m*	3.50 t (8.4)	3.51 m*
3	3.32 m*	3.46 m *	3.46 m*	3.52 m*	3.38 m*	3.70 m*	3.35 t (9.2)	3.33 m *	3.35 m*
4	3.11 t (7.2)	3.52 m *	3.41 m*	3.40 m*	3.19 m*	3.40 m*	3.22 t (9.6)	3.17 t (9.0)	3.20 m*
5	3.40 m*	3.99 m *	3.90 m*	3.30 m*	3.73 m*	3.30 m*	3.48 m*	3.70 m *	3.69 m*
6a	3.17 m*	4.26 m *	4.20 m *	3.70 m*	3.88 dd (12.0, 6.6)	3.40 m*	3.54 m*	4.35 d (10.8)	3.96 m *
6b	3.03 m*	4.39 d (12.0)	4.35 m *	3.70 m*	4.36 m*	3.40 m*	3.74 d (12.0)	3.88 m	4.35 d (11.9)
Glc D (R_5)									
1		4.27 d (7.1)	4.26 d (7.6)	4.26 d (7.8)					
2		3.00 t (7.1)	3.00 m*	3.58 m*					
3		3.18 m *	3.16 m*	3.52 m*					
4		3.06 m *	3.09 m*	3.40 m*					
5		3.27 m *	3.25 m*	3.35 m*					
6a		3.43 m *	3.41 m*	3.70 m*					
6b		3.71 m *	3.69 m*	3.70 m*					
Feruloyl (R_1)									
2		6.97 s	7.16 s	7.00 s	6.97 s		7.05 s	6.98 s	7.07 s
5		6.70 d (7.2)	6.75 d (8.4)	6.88 d (7.2)	6.71 d (9.0)		6.76 d (8.2)	6.69 d (8.4)	6.72 d (8.4)
6		6.90 m *	6.99 d (8.0)	6.70 d (7.8)	6.87 d (8.4)		6.95 d (8.0)	6.88 d (7.8)	6.89 m*
α		6.24 d (15.6)	6.37 d (15.6)	6.23 d (16.2)	6.24 d (16.2)		6.24 d (15.9)	6.25 d (16.2)	6.10 d (15.9)
β		7.33 d (16.2)	7.45 d (15.6)	7.32 d (15.6)	7.32 d (16.2)		7.33 d (15.7)	7.34 d (15.6)	7.19 d (15.9)
3-OCH_3		3.71 s	3.77	3.74 s	3.69 s		3.74 s	3.68 s	3.75 s
Feruloyl (R_2)									
2	6.86 m*			7.04 s					7.07 s
5	6.72 d (7.8)			6.72 d (7.8)					6.71 d (8.0)
6	6.91 d (8.4)			6.84 d (7.8)					6.87 m*
α	6.22 d (15.6)			6.08 d (15.6)					6.24 d (15.7)

β	7.30 d (15.6)			7.17 d (15.0)					7.35 d (15.5)
3-OCH_3	3.70 s			3.71 s					3.71 s
Sinapoyl or feruloyl (R_3)									
2	6.88 s	6.91 s	6.95 s		6.91 s	6.87 s	6.96 s		
5			6.67 d (8.4)						
6	6.88 s	6.91 s	6.87 d*		6.91 s	6.87 s	6.96 s		
α	6.40 d (15.6)	6.46 d (15.6)	6.24 d (16.0)		6.44 d (16.2)	6.40 d (16.0)	6.46 d (15.7)		
β	7.42 d (15.6)	7.43 d (16.2)	7.30 d (15.6)		7.46 d (16.2)	7.42 d (16.0)	7.47 d (16.4)		
3-OCH_3	3.75 s	3.78 s	3.69		3.78 s	3.76 s	3.79 s		
5-OCH_3	3.75 s	3.78 s			3.78 s	3.76 s	3.79 s		
Malonoyl (R_4)									
CH_2		3.30 s *	3.27 s	3.30 s	3.34 s			3.33 s	3.37 s

[a] Values in parentheses indicate coupling constants (*J* in Hz)
[*] Overlapped signals

Table 3. ^{13}C NMR spectroscopic data of anthocyanins isolated from *R. sativus* cv. *Sango* sprouts in DMSO-d_6 : TFA-d_1 (9:1) . Signals were indirectly detected by HSQC and HMBC analysis.

	1	**2**	**3**	**5**	**7**	**8**
Aglycon						
2	167.7	162.7	162.5	162.5	162.6	162.6
3	145.9	144.9	144.9	144.6	144.7	144.9
4	135.5	130.7	131.9	131.7	132.0	131.3
4 a	112.5	111.7	111.8	111.6	111.5	111.9
5	154.6	155.0	155.1	155.1	155.2	155.1
6	112.3	104.5	104.8	104.4	104.7	104.7
7	168.5	167.8	167.8	167.3	167.8	167.5
8	96.5	96.1	94.6	96.0	96.2	96.2
8 a	155.4	155.7	155.6	155.1	155.2	155.0
1’	119.5	120.0	120.1	119.9	120.1	119.7
2’	117.8	116.8	117.2	117.1	117.2	117.5
3’	147.5	147.2	147.3	146.7	146.9	146.6
4’	155.1	155.8	155.3	155.6	155.7	155.4
5’	117.6	117.2	117.3	116.8	117.0	116.9
6’	129.2	129.2	128.8	128.6	128.7	127.7
Glc A						
1	99.4	96.8	98.4	98.8	98.8	99.1
2	78.3	77.2	77.3	77.5	77.5	80.8
3	76.0	76.3	76.4	76.5	76.3	76.0
4	69.8	70.1	70.1	70.2	70.1	75.8
5	74.5	73.3	72.7	73.7	73.8	73.7
6	62.1	63.5	64.1	63.2	62.7	63.1
Glc B						
1	100.4	99.7	99.3	99.6	99.9	103.6
2	74.8	73.8	74.3	74.1	74.0	74.5

3	78.5	79.9	75.1	74.8	74.7	76.0
4	71.5	70.4	71.1	70.7	70.8	69.5
5	74.5	77.5	77.8	77.5	77.7	76.7
6	62.0	61.3	61.5	61.3	61.0	60.6
Glc C						
1	102.5	101.2	101.4	101.5	102.2	101.5
2	74.2	72.8	74.6	73.0	73.4	72.9
3	76.9	74.8	79.7	75.8	76.2	76.5
4	70.5	70.1	70.2	69.6	69.9	69.8
5	78.1	72.1	74.2	74.3	77.8	74.1
6	62.1	62.5	63.4	64.2	61.0	64.1
Glc D (R_5)						
1		103.4	103.8			
2		73.5	73.5			
3		76.3	70.4			
4		70.1	70.0			
5		76.6	77.3			
6		61.1	61.6			
Feruloyl (R_1)						
1		126.0	126.2	125.8	125.7	125.7
2		111.6	111.4	111.7	111.8	111.8
3		148.4	148.4	148.0	148.3	148.0
4		147.9	148.1	149.7	149.3	149.6
5		115.6	115.9	115.6	115.8	115.5
6		123.0	123.4	123.1	123.2	122.9
α		114.2	115.3	114.0	115.7	113.9
β		149.5	145.6	145.6	145.7	145.4
3-OCH_3		55.8	56.1	55.7	55.9	55.6
CO		166.8	166.7	166.2	166.9	166.9
Feruloyl (R_2)						

1	125.2					
2	116.5					
3	147.6					
4	149.5					
5	116.0					
6	123.8					
α	114.6					
β	146.2					
3-OCH_3	55.6					
CO	165.6					
Sinapoyl or feruloyl (R_3)						
1	125.5	124.9	124.8	125.0	124.9	
2	107.1	106.3	112.0	106.7	106.4	
3	147.9	148.5	148.4	148.4	138.6	
4	107.1	139.9	140.2	145.5	148.5	
5	147.9	148.5	116.2	148.4	138.6	
6	106.5	106.3	123.1	106.7	106.4	
α	116.3	115.5	114.2	115.6	115.8	
β	145.8	145.8	146.0	145.2	145.4	
3-OCH_3	56.1	56.0	56.1	56.2	56.4	
5-OCH_3	56.1	56.0		56.2	56.4	
CO	166.3	166.2	166.3	166.2	166.2	
Malonoyl (R_4)						
1		166.7	167.7	167.0		167.0
2		41.1	41.4	41.2		41.1
3		168.3	167.7	168.3		168.3

Table 4. Rate constants and stoichiometric factors for reaction with peroxyl radicals of anthocyanins from *R. sativus* cv. *Sango* sprouts, their acylating phenolic acids and corresponding esters, and reference compounds, determined from the inhibited autoxidation of styrene and cumene in acetonitrile (containing 1% v/v formic acid) at 30°C.

					$10^{-5} \bullet k_{inh}$ (in styrene)		*n*	
id	**R_1**	**R_2**	**R_3**	**R_4**	**Inhibited** [a]	**Retarded** [a]	**(styrene)**[b]	**(cumene)**[b]
5	feruloyl	H	sinapoyl	malonoyl	2.0±0.2	0.40±0.10	3.5±0.4	6.8±0.6
7	feruloyl	H	sinapoyl	H	1.9±0.2	0.35±0.05	3.7±0.2	6.3±0.5
8	feruloyl	H	H	malonoyl	0.9±0.2	0.34±0.06	1.8±0.2	4.0±0.5
9	feruloyl	feruloyl	H	malonoyl	1.2±0.2	0.34±0.07	2.2±0.1	5.7±0.6
Methyl Sinapate					1.8±0.4		1.9±0.3	
Sinapic acid					1.6±0.2		2.1±0.2	
Ethyl Ferulate						0.4±0.1		(2.0)[c]
Ferulic acid						0.3±0.1		2.0±0.2
Cyanin						0.4±0.2		3.0±0.5
Tocopherol					6.0±1.0		2.0±0.1	

[a] Determined, respectively, from the slope of inhibited period and retarded period in the autoxidation of styrene. Refer to text and figure 2.
[b] Stoichiometric factor measured in the autoxidation of the substrate indicated in parenthesis
[c] Not determined. In parenthesis is indicated the expected value based on the measured value of ferulic acid.

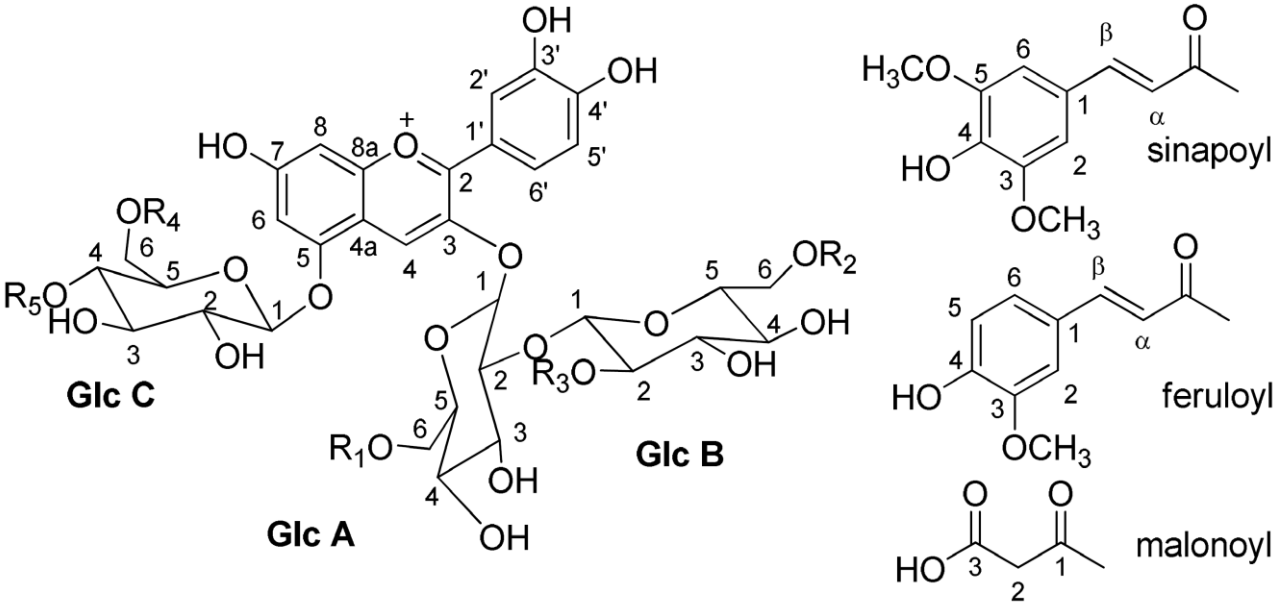

ID	R_1	R_2	R_3	R_4	R_5
1	H	feruloyl	sinapoyl	H	H
2	feruloyl	H	sinapoyl	malonoyl	β-glucose
3	feruloyl	H	feruloyl	malonoyl	β-glucose
4	feruloyl	feruloyl	H	malonoyl	β-glucose
5	feruloyl	H	sinapoyl	malonoyl	H
6	H	H	sinapoyl	H	H
7	feruloyl	H	sinapoyl	H	H
8	feruloyl	H	H	malonoyl	H
9	feruloyl	feruloyl	H	malonoyl	H

Figure 2. Structures of the anthocyanins isolated from *Raphanus sativus* cv. Sango sprouts.

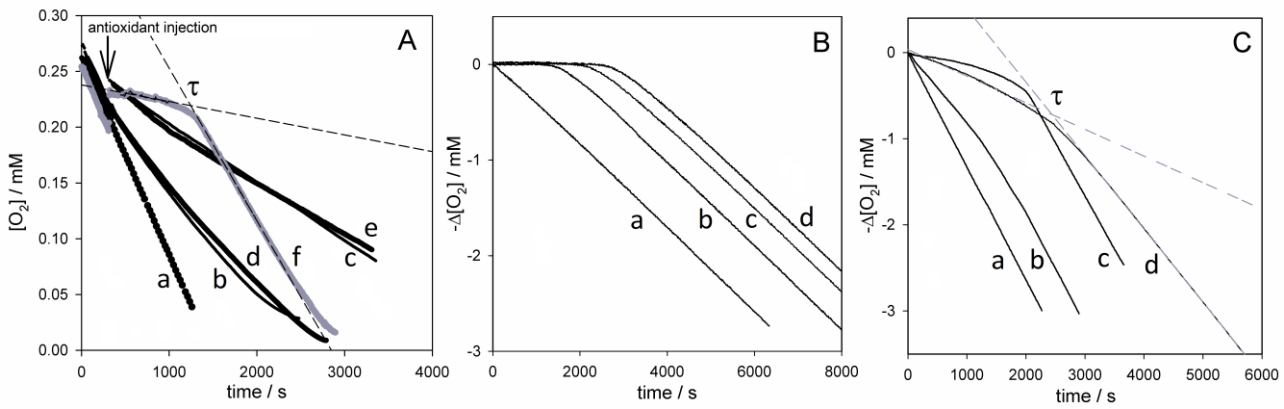

Figure 2. Oxygen uptake kinetics during the controlled autoxidation of: A) 30 mM linoleic acid in Triton-X100 (0.16 M) neutral micelles at 37°C without inhibitor (a), or inhibited by: anthocyanin **1**, 4.0 μM (b), or 8.0 μM (c); anthocyanin **3**, 4.0 μM (d), or 8.0 μM (e); 3.3 μM α-tocopherol (f); B) 1.7 M cumene in acetonitrile at 30°C without inhibitor (a), or inhibited by: 5.5 μM anthocyanin **8** (b); 4.5 μM anthocyanin **7** (c); 3.9 μM anthocyanin **5** (d). C) 2.1 M styrene in acetonitrile at 30°C without inhibitor (a), or inhibited by: 5.0 μM Ethyl ferulate (b); 6.0 μM α-tocopherol (c); 4.2 μM anthocyanin **7** (d). Dashed lines represent linear regressions of the inhibited and subsequent portion of autoxidation; τ indicates the inhibition time.